Chapter 2

Tunable Graphene Based Metasurface for Polarization-Independent Broadband Absorption in Lower Mid Infrared (MIR) Range

2.1. Introduction

Absorbers have generated great interest among researchers to find their potential applications towards spectroscopy, sensing etc [165]. With the introduction of concept of metastructures, ultra-thin compact absorbers have been designed and developed in different frequency regions ranging from microwave to optical bands [166]-[167]. But, these structures cannot be able to absorb over a wide frequency band because of high Q of the resonating nature of the metastructure [168]-[169]. Incorporation of lumped elements have been reported to enhance the absorption bandwidth; but they are very difficult to realize in practice as well as the structures lose the inherent advantage of using metastructures like compact, ultra-thin and light weight [170].

Recently semi-metals and graphene have been introduced in the metasurface design to tune the absorption bandwidth where the conductivity can be modulated by control of chemical doping or mechanical stretching [171]-[175]. Till date, narrowband absorption for single band and multiband designs by using graphene metasurface has been reported [176]-[181]. Graphene nanosheets were incorporated and suspended with organic compounds in a paint form to utilize it as radar absorbing materials at X-band [182]. Wideband absorption has been achieved by using several layers of dielectric materials, multiple layers of graphene and the combination of

the two. However, they possess considerable thickness; thus, sacrificing the basic advantage of ultra-thin nature of the metasurface. Recently, wideband absorption has been implemented by using composite dielectric metasurface as well as by using multilayer graphene metasurface [179], [183]. Broadband absorption has also been achieved using stack of graphene-dielectric multilayer structures; however, the thickness of the structures is quite high as well as they are difficult to fabricate [184]-[186]. These types of structures too suffer from thickness issue. These types of designs provide wide absorption bandwidth but they are difficult to fabricate. The absorption of the graphene based metasurface structures has also been analyzed in the light of circuit theory approach. Polarization-independent absorption can be attained by the deposition of specific graphene pattern on the top surface of dielectric-metal stacked structure in the terahertz regime [186]. Due to the discrete distribution of graphene energy level in the periodic environment, it is highly challenging to control the electronic properties of graphene metasurface [173]-[175]. However, the Fermi level of graphene can be directly controlled by impurity doping profile as well as mechanical straining [187]-[190].

Researches on millimeter-wave and higher frequency bands have been explored to study the growth of demand of data to pave the way towards 5G-communication system [191]. To allow higher data rates, improved physical security and avoiding electromagnetic interference, researches towards optical wireless communication have been potentially increased nowadays [191]-[193]. Avoiding electromagnetic interference is an important integral part of EMC. Terahertz gap (0.1-10 THz) can serve as a bridge between mm-wave and optical spectrum where naturally available materials cannot be used as they suffer from high loss [194].

In this chapter, a broadband absorber has been realized using single layer of graphene based metasurface structure deposited over ultrathin metal-backed dielectric. Broadband absorption has been obtained by creating a square fractal slot structure from the graphene layer. It is observed that absorptivity is nearly unity at 4.21 THz, 6.78 THz and 9.27 THz. The unit cell

contains a fractal shaped slot structure, which has been etched out from the square shaped graphene layer grown over amorphous SiO_2. Later, a square graphene pattern has been deposited within the previously said slotted area to improve coupling and absorption bandwidth. The whole shape is maintained in single unit cell.

The design produces a wide absorption bandwidth of 6.08 THz using only a single layer (2D) graphene construction on the amorphous silicon dioxide (SiO_2) substrate backed by 0.1 μm thick layer of gold. Considering the periodicity and thickness the presented absorber is ultra-thin in nature with respect to the previously reported manuscripts. The proposed structure is purely insensitive to the orientation of the electric field vector of the electromagnetic wave incident on the top surface of the absorber over broad bandwidth of 6.08 THz. Under TE and TM polarizations, the design provides enhanced electromagnetic absorption bandwidth up to 40^o incident angles.

Metasurface plays a vital role in controlling electromagnetic (EM) wave and diversifies into several applications, such as absorbers, polarizers, cloaking, sensors, and many more [195]-[197]. Recently the research in terahertz gap (0.1 THz -10 THz) lying in the transition bands of the mm-wave and optical region have generated interest due to the availability of high bandwidth and allocation of several users [198]-[199]. Electromagnetic wave (EM) absorbers using metasurfaces have been reported employing metallic sub-wavelength structures in the microwave and millimeter-wave range [200]-[201]. However, narrow absorption bandwidth due to the high-quality factor of the resonating nature of the metasurface appears as a drawback to these structures [202]. Some of the recent studies have indicated that the incorporation of lumped elements to enhance absorption bandwidth; however, they are quite difficult to realize in practice and contradict to the ultra-thin concept [203]. Recently, atomically-thin two-dimensional (2D) graphene-based metasurfaces have attracted huge research attention owing to the controllability of graphene's conductivity, which helps in developing various

metasurface related structures in THz frequency regions [204]-[206]. Several literatures presented about narrow-band and multi-band absorbers with graphene metasurface [207]-[208]. Narrowband, as well as broadband absorption in the terahertz region, has been achieved using monolayer graphene and multiple graphene metasurface or multiple dielectric layers or the combination of both which are very unreliable and extremely difficult to fabricate [209]-[212]. Double-layer graphene metasurface with less substrate thickness can be a better solution to the multilayered structures as this arrangement provides wider absorption bandwidth with high reliability, smoother fabrication, and safety with the better performance [213]-[214]. Several theories and explanations are available in several literatures, which validate the working principle of metasurface absorber [215]-[216]. Most of the metasurface absorbers have been implemented employing two-fold symmetry or four-fold symmetric resistive graphene pattern on the top surface (EM wave interaction surface) of the substrate so that overall device can deliver polarization-independent absorption [217]. Control of the electronic properties of graphene is highly challenging because of the discrete distribution of graphene energy level in the periodic boundary conditions [218]. Fermi level of graphene can be adjusted according to the requirements by external doping of impurities or mechanical straining of the graphene layer [219]-[221].

The proposed absorbers can also be used to realize compact antenna test range for target detection as well as implementing of terahertz biosensors, which mostly emphasize on improving the sensitivity by maximizing changes in resonance frequency in terms of deposited film and thereby can be used as a promising application for 5G wireless communications and beyond [222]-[223].

2.2. Design and Simulation of Structure

The schematic diagram of the graphene based metasurface has been presented in Fig. 1. The whole package contains three layers consisting of top graphene layer (thickness, t_g =0.001 µm), 0.1 µm thick (t_{gold}) gold bottom layer of electrical conductivity (σ) of 4.56×107 S/m and 7 µm thick (t_{SiO2}) amorphous silicon dioxide (SiO_2) layer of effective dielectric constant of 2.1 with loss tangent (tan δ) of 0.0006 sandwiched between them. At the optical frequency range, the skin depth of most of the metals is approximately equal to 0.05 µm. The top layer composes of an array of periodic pattern of the structure presented in the unit cell. The proposed monolayer graphene pattern is oriented along *xy*-plane. The open boundary is along the *z*-direction to allow the electromagnetic wave incident to the structure. The top view and 3-D perspective view of unit cell element of the presented metasurface design are shown in

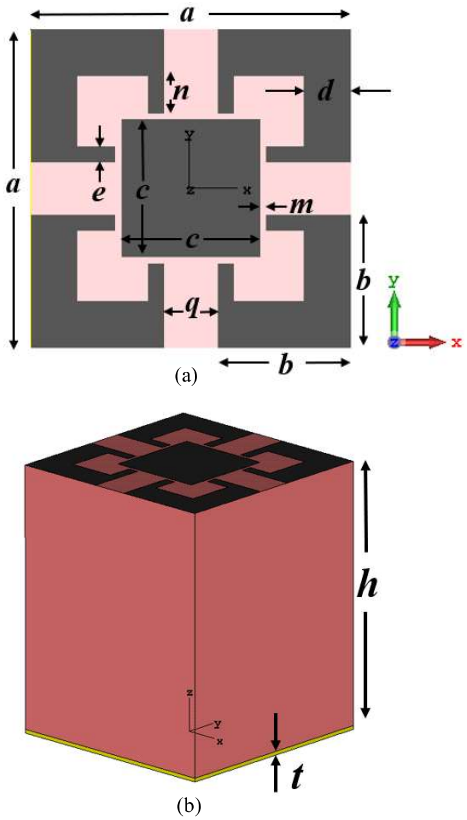

Fig. 2.1. (a) Top view and (b) 3-D perspective view of the wideband graphene-based metasurface absorber in lower MIR region.

Fig. 2.1.(a) and Fig. 2.1.(b), respectively. The geometrical dimensions of the unit cell depicted in Fig. 2.1.(a) and Fig. 2.1.(b) are parametrically optimized as, periodicity a = 6 μm, where the other dimensions are q = 1 μm, d = 1 μm, n = 1 μm, c = 2.6 μm, b = 2.50 μm. CST MWS software tool is used for the simulation of the proposed design. CST Microwave Studio is an electromagnetic simulator based on FIT, which provides spatial discretization method applicable to several electromagnetic problems from static field calculations to high frequency applications in time domain as well as in frequency domain [224]-[226].

In the proposed design, the three-layered unit cell is designed in CST by proper assignments of metal using Drude model and dielectric. The graphene layer is designed by incorporation of complex conductivity given by Kubo's formula and oriented along *xy*-plane [227]. Floquet boundary conditions are assigned in the designed unit cell to realize an infinitely long array in *xy*-plane. The normal plane wave (EM wave) incidence takes place along the z-axis. The structure is surrounded by perfectly matched layer (PML) from all sides so that waves scattered from edges gets absorbed. In the floquet boundary option two modes are selected to check the

Table 2.1. Brief Description of Simulation Results

Simulation Input	Effect on Output
Linearly polarized plane wave incident on the top surface of the designed absorber	Circulating current loop is formed between top surface and bottom surface of the overall structure which forms magnetic excitation.
Graphene metasurface (t_g = 0.001 μm, T = 300 K, μ_c = 1 eV, τ = 0.067 ps, a = 6 μm, q = 1 μm, d = 1 μm, n = 1 μm, c = 2.6 μm, b = 2.50 μm) All the parameters are described in the manuscript.	Working as a matching circuit for air medium and SiO_2.
Silicon Dioxide (SiO_2) substrate (ε_r = 3.9, tan δ= 0.0006, t_{SiO2} = 7 μm) All the parameters are described in the manuscript.	Acting as the medium where multiple reflections of the EM wave are taking place and the reflection loss is stored as EM wave absorption.
Gold metal background ($\sigma_{elect.}$ = 4.56×10^7 S/m, t_{gold} = 0.1 μm) All the parameters are described in the manuscript.	Acting as a reflector which forbids the transmission of the EM wave.

performance of the graphene-based metasurface for oblique incidences under both transverse electric (TE) and transverse magnetic (TM) polarizations. The frequency range has been assigned as per terahertz range calculation and the dimensions are taken in micrometers (μm). The package is analyzed methodically in the frequency domain solver to calculate reflection (r) and transmission (t) characteristics. In optical frequencies, skin depth is negligible in comparison with a conductor's thickness. Thus, the incident electromagnetic wave undergoes complete reflection from the top surface of bottom gold layer of 0.1 μm thickness as it exceeds the skin-depth at the frequency of operation, thereby leading to zero transmission. Here, the absorption is completely dependent on reflectivity, can be enhanced by reducing the reflection from the surface. So, the electromagnetic wave is reflected back from the bottom gold layer

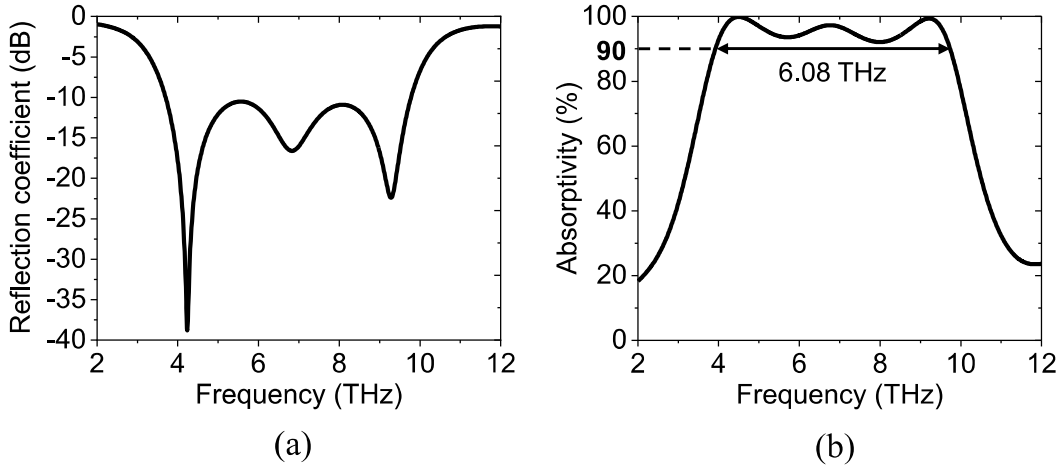

Fig. 2.2. Frequency responses of (a) reflection coefficient of the designed absorber and (b) absorptivity.

although it is 0.1 μm thick. As the transmission coefficient is zero, the absorptivity can be evaluated from $A = 1 - |r|^2$, where A is absorptivity and $|r|^2$ is reflectivity of the wave incident on the top surface of the design. The reflectivity curve is presented in Fig. 2.2(a) and the corresponding absorptivity curve is also shown in Fig. 2.2(b). It is seen from Fig. 2(a) that the reflectivity level is less than -10 dB within the frequency band 3.69 THz to 9.77 THz as evident from Fig. 2.2(b). This gives rise to fractional bandwidth ~90.34% with respect to the centre

frequency of proposed absorption band with more than 90% absorptivity. Three distinct minima have been realized at 4.21 THz, 6.78 THz and 9.27 THz in terms of local and global minima concept as evident from the reflectivity response (Fig. 2.2(a)). The reflectivities at 4.21 THz, 6.78 THz and 9.27 THz are -37 dB, -18 dB and -23 dB giving rise to respective absorptivities of 99.9 %, 97 %, and 99.4 %.

The electrical conductivity of graphene plays a major role in perfect wideband absorption of electromagnetic wave in MIR region. Graphene is defined as an anisotropic medium in the CST simulator. Electromagnetic wave is incident upon the proposed absorbing metasurface at different angles including the normal incidence. The situation can be described as an interface between two dielectric materials (air and SiO_2) and graphene metasurface structure is placed in between them acting as a matching circuit so that incident EM wave can propagate through the silicon dioxide material [228]. At the back of the SiO_2, a thin gold metal plate is placed and for this the EM wave cannot be able to transmit through the package. Consequently, the EM wave is absorbed at the maximum amount. Impedance matching theory helps to understand EM wave absorption by a metasurface [229].

2.3. Simulated Results and Discussions

The proposed graphene metasurface has four equivalent parts separated in a uniform manner to make a square fractal like slot. A square size layer of graphene is deposited within that fractal like slot to increase coupling between the earlier said four equivalent distinctively designed graphene layer parts and the square size graphene layer. The geometrical dimensions of the fractal shaped slots are parametrically analysed so that enhanced absorption over lower MIR region can be obtained. The absorptivity response of this structure has been discussed with respect to the variations of different geometrical dimensions involved. The authors changed one parameter at a time without changing rest of the parameters and the performances had been shown in different parametric variation graphs plotted in the manuscript. For example, in Fig.

2.3(a), parametric variation of q has been performed from 0.5 µm to 1.1 µm keeping the other parameters *viz.*, a, b, c, d, e, m, n and h constant. The gap (q) between the symmetric

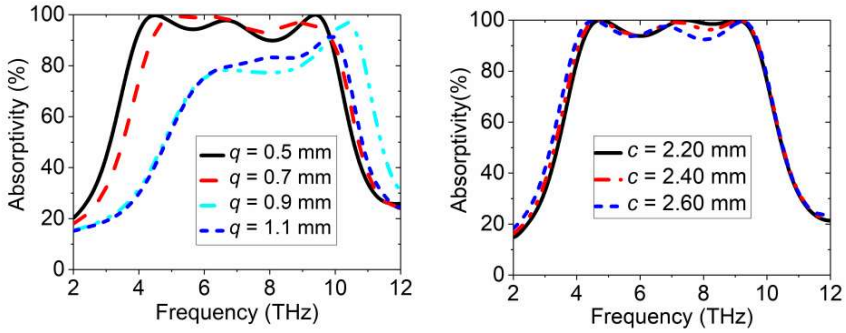

Fig. 2.3. Frequency responses of the parametric variations of (a) gap between symmetric elements (q) and (b) dimension of the square shaped graphene layer in the middle of the slotted area (c).

elements of the graphene meta-structure has been varied to modulate the capacitance generated between the symmetric elements, which in turn change the frequency of absorption. The blue-shift of the absorptivity curve is thus observed in Fig. 2.3(a). Next the dimensions (c) of the square size graphene layer in the middle of them are varied to optimize the coupling between the symmetric elements and the square size graphene layer. The best performance is derived in the graph in Fig. 2.3(b) when c = 2.20 µm in terms of absorption peak and c = 2.60 µm in terms of bandwidth. The coupling can be improved by changing the length of the narrow arms (n) and it is another way of representation of the coupling variation between the four symmetric graphene layer parts and the aforementioned square graphene layer placed in the middle.

The designed graphene based metasurface package is examined under different heights of the amorphous silicon dioxide shown in Fig. 2.4(a). The increase in substrate thickness causes confinement of more energy within the dielectric and thereby the absorption bandwidth gets enhanced. The best performance can be observed from Fig. 2.4(a) with the maximum absorption having three absorption peaks within the whole bandwidth. Absorptivity response has also been observed for different periods (a) of the unit cell. As the period is increased, the

gap between the neighbouring graphene metasurface structures increases. The absorption band undergoes complete blue-shift band as the equivalent fringing capacitance is decreased. This can be experienced from Fig. 2.4(b). The variations in bandwidth in Fig. 2.4(b) have been occurred due to change in coupling strength between resonating parts of the structure.

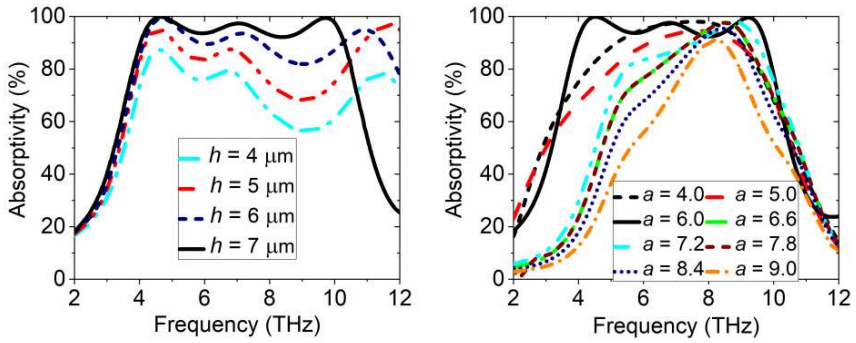

(a) (b)

Fig. 2.4. Variation of absorptivity (a) due to the change in substrate thickness (h) and (b) change in periodicity (a) of the unit cell.

Now, the graphene pattern shape is changed parametrically. As the shape is decreased, the interaction area between the top graphene layer and the immediate bottom dielectric material has also been deteriorated. The surface conductivity of graphene layer has been decreased. The gradual decrease in absorptivity can be viewed from Fig. 2.5(a) as absorptivity is directly related to the graphene's surface conductivity. The next encounter is about the thickness variation of the principal arm of the symmetric graphene structures. The absorptivity response due to this change is seen from Fig. 2.5(b) and the reason behind this response can be explained like the previous concept.

The relaxation time (τ) has been varied to check the absorptivity performance of the designed prototype depicted in Fig. 2.6(a). τ affects the plasmon propagation distance in graphene-SiO_2 interaction. Graphene exhibits larger confinement when light-matter interaction occurs with the silicon dioxide interface compared to noble metals. The tunability of the graphene layer can be achieved by the control of chemical potential of the graphene layer [230]. Plasmon

propagation distance of the graphene layer is inversely proportional to τ [230]. To increase the plasmon propagation distance τ has to be reduced. Some previous literatures used the reduced values of relaxation time (τ) up to a certain level [230]-[231] to check the optimized performance of graphene plasmons. The best performance is provided by the absorber when τ = 0.06 ps as this time duration is the longest duration between the two consecutive collisions of the electrons in this experimental simulation. At this value the conductivity of the graphene layer will be the highest. The absorption bandwidth is also found to be maximum at τ = 0.06 ps as shown in Fig. 2.6(a). Normally, chemical potential (μ) is applied in between the graphene metasurface and the bottom gold layer. Chemical potential (electric potential) is also an important parameter to tune the Fermi energy of graphene. The variations of chemical potential in the manuscript are realistic and it can be validated from [231]. The spatial structure and thickness of graphene layer are significant to the performance of the proposed metasurface absorber structure. Shaping of the graphene structure in different dimensions results in tailoring the localization of mid-infrared electromagnetic fields at nanoscale [232]. The absorptivity bandwidth variation for different chemical potential values has been demonstrated in Fig. 2.6(b). Both the width and height of the absorption curve is increased with the increment of the μ values as the chemical potential is a function of the

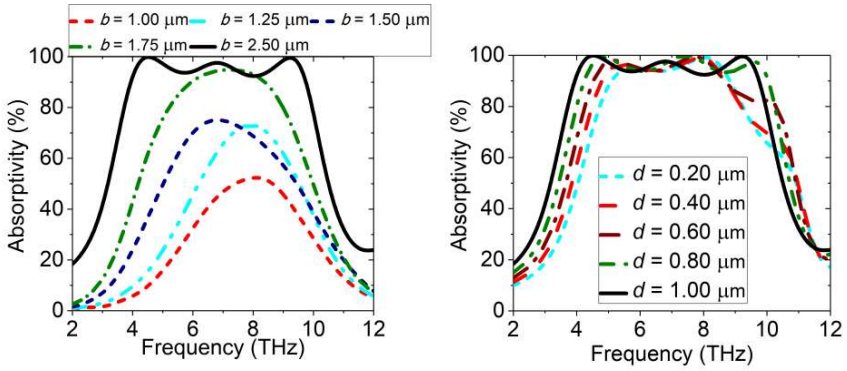

Fig. 2.5. Absorptivity variations under (a) overall size of graphene layer (b) along with (b) the thickness (d) of the principal arm of the symmetric graphene layer.

conductivity of graphene. The chemical potential μ will increase for the larger values of Fermi energy (E_f). Therefore, increase in E_f increases the conductivity of the graphene layer (σ_g) as determined from Chapter 1. The absorptivity response is blue-shifted when μ = 1 eV and it is red-shifted when μ = 0.2 eV with least absorption. Now graphene's permittivity can be modified by the chemical potential (μ) related indirectly as it is dependent on graphene's conductivity, the absorptivity is changing accordingly. Absorption gets increased with the increase in permittivity due to change in chemical potential and hence the designed prototype can have application towards permittivity sensing [227]. This way tunability property has been achieved in graphene based metasurface and the absorption band can be tuned to different frequency ranges.

The proposed structure is studied under various polarization angle (ϕ) whose response is shown in Fig. 2.7(a). It is found that the frequency response of the structure remains invariant with respect to the polarization angle. The absorptivity responses of the structure are also studied for different incident angles under both TE and TM polarizations as illustrated in Fig. 2.7(b) and Fig. 2.7(c) respectively. The structure shows 99.99% to 80% absorptivity with respect to

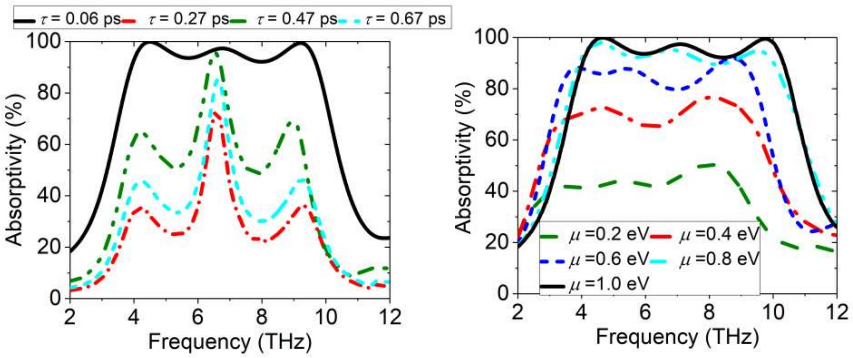

Fig. 2.6. Responses of absorption bandwidth (a) under different relaxation time (τ) and (b) by applying different chemical potential (μ).

normal incidence (θ = 0º) to oblique incidence (up to θ = 40º) with the three resonance peaks at 4.21 THz, 6.78 THz and 9.27 THz in accordingly. The high absorptions at 4.21 THz, 6.78

THz and 9.27 THz have been explained in the light of calculated electromagnetic parameters as well as the field distributions. The effective permittivity (ε_{eff}) and effective permeability

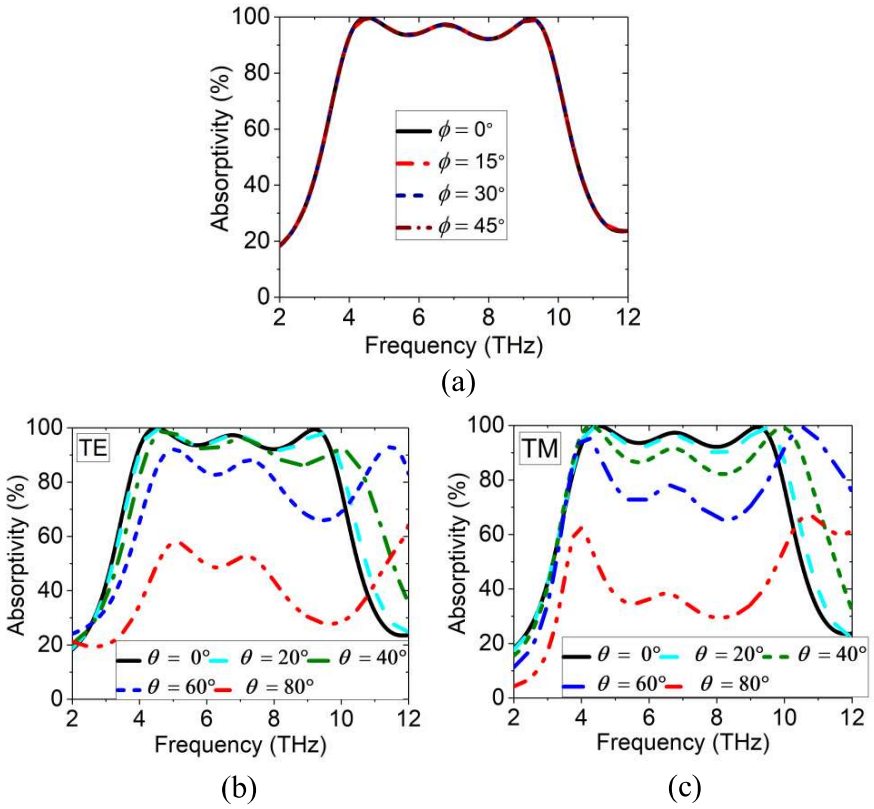

Fig. 2.7. Responses of the wide absorption bandwidths under (a) different polarization angles (ϕ), and different incident angles (θ) for (b) TE polarization and (c) TM polarization.

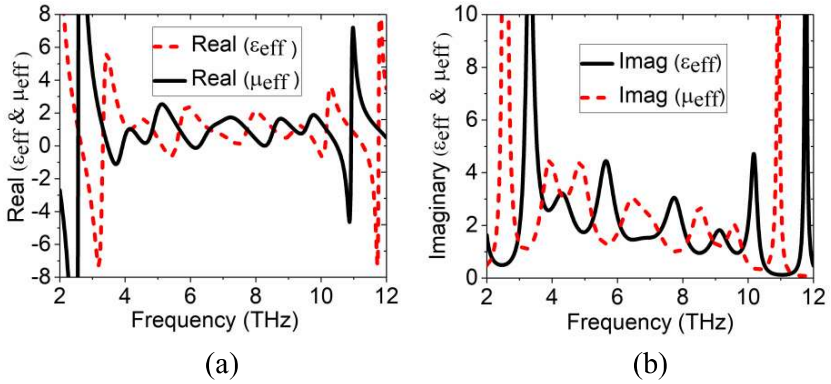

Fig. 2.8. Frequency responses of (a) real values of ε_{eff} and μ_{eff} (b) imaginary values of ε_{eff} and μ_{eff}.

(μ_{eff}) are calculated using equation (2.1) where d is the distance travelled by the incident wave and k_0 is the propagation constant of the wave at free space. The calculated values of the constitutive parameters are tabulated in Table I for three major absorption peak frequencies

$$\chi_{es} = \frac{2j}{k_0}\frac{1 - S_{11}}{S_{11} + 1}$$

$$\chi_{ms} = \frac{2j}{k_0}\frac{S_{11} + 1}{1 - S_{11}}$$

$$\varepsilon_{eff} = 1 + \frac{\chi_{es}}{d}$$

$$\mu_{eff} = 1 + \frac{\chi_{ms}}{d} \qquad (2.1)$$

Table 2.2. Calculation of Constitutive Parameters

Frequency (THz)	Real Part		Imaginary Part	
	ε_{eff}	μ_{eff}	ε_{eff}	μ_{eff}
4.21	1.02	0.98	3.13	3.34
6.78	0.90	1.18	1.53	2.34
9.27	1.11	0.91	1.61	1.33

viz. 4.21 THz, 6.78 THz and 9.27 THz. In these three frequencies real and imaginary parts of ε_{eff} and μ_{eff} of the effective medium are almost equal suggesting the matching of impedance between the absorber and free space have taken place. The extracted values of the above said constitutive parameters are plotted in graphs in Fig. 2.8(a) and Fig. 2.8(b).

To clarify the absorption mechanism of the designed prototype, the electric field distributions are investigated at these three different frequencies. The electric field distributions are dense at the edges of the horizontally slot of the graphene layer at 4.21 THz as represented in Fig. 2.9(a). At 6.78 THz the E-field gets distributed at both the edges of the horizontal and vertical slots of the graphene layer as shown in Fig. 2.9(b). At 9.27 THz electric fields are concentrated on both the edges of the horizontal and vertical slots of the graphene metasurface as depicted from Fig. 2.9(c).

The surface current distribution patterns are shown in Fig. 2.10(a) for the top graphene metasurface and in Fig. 2.10(b) for the bottom gold plane. The surface currents are shown at 4.21 THz, 6.78 THz and 9.27 THz respectively. In the first two frequency bands the top and bottom surface current distribution vectors are anti-parallel involving magnetic dipole excitation in terms of resonance. On the other hand, at the highest frequency band (9.27 THz),

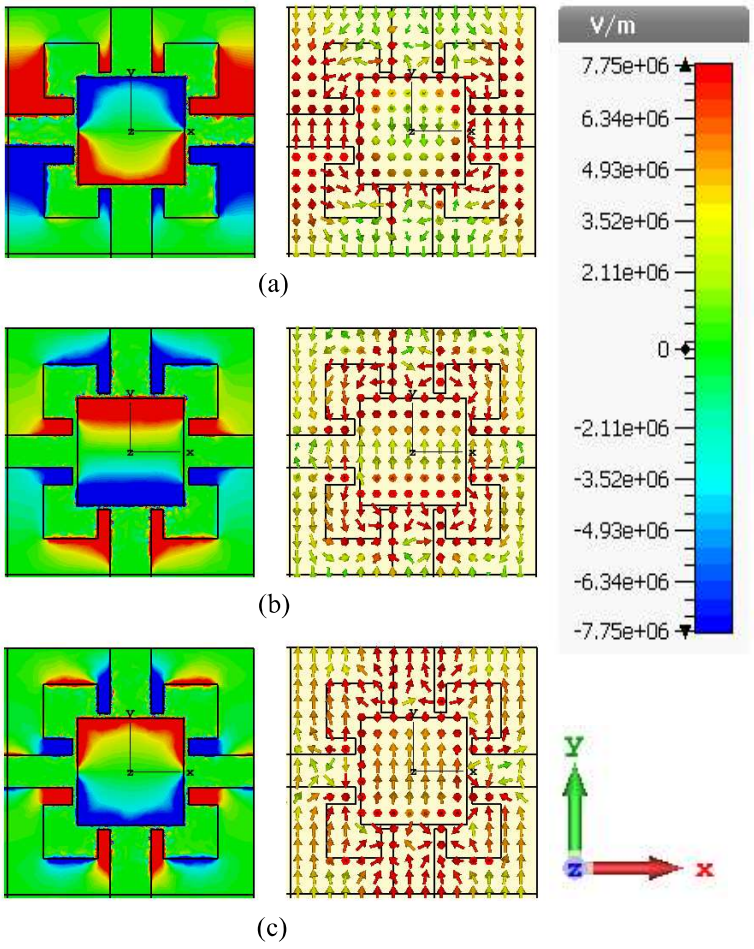

Fig. 2.9. (a) Electric field distributions at (a) 4.21 THz, (b) 6.78 THz and (c) 9.27 THz.

the top and bottom surface current distribution vectors are parallel to each other giving rise to the induced electric resonance. This way, both the electric resonance and the magnetic resonance cause high absorption at the three distinct frequencies. The power loss patterns lie on the similar regions of the absorber like the E-field distributions at the above said three different frequencies. In order to have more clear view about the genesis of the coupling effect

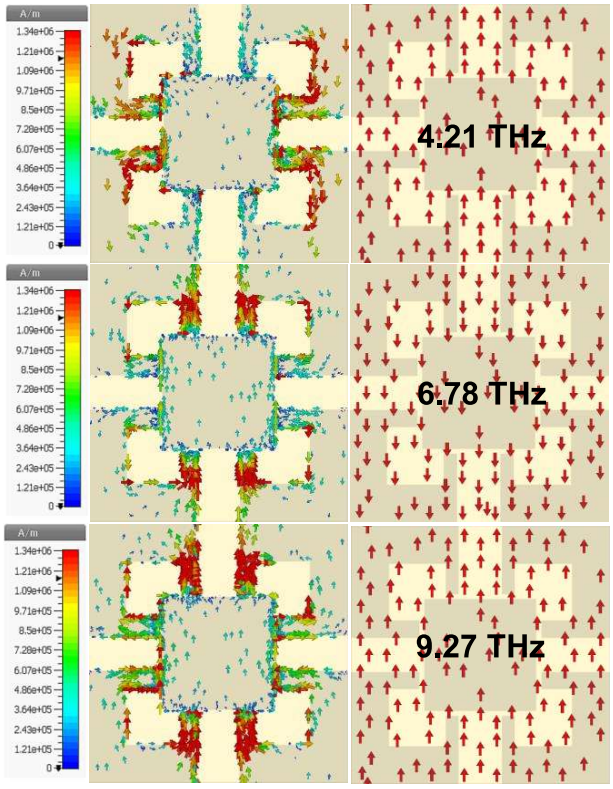

Fig. 2.10. (a) Surface current distributions for (a) top layer and (b) bottom layer of proposed metasurface structure at 4.21 THz, 6.78 THz and 9.27 THz.

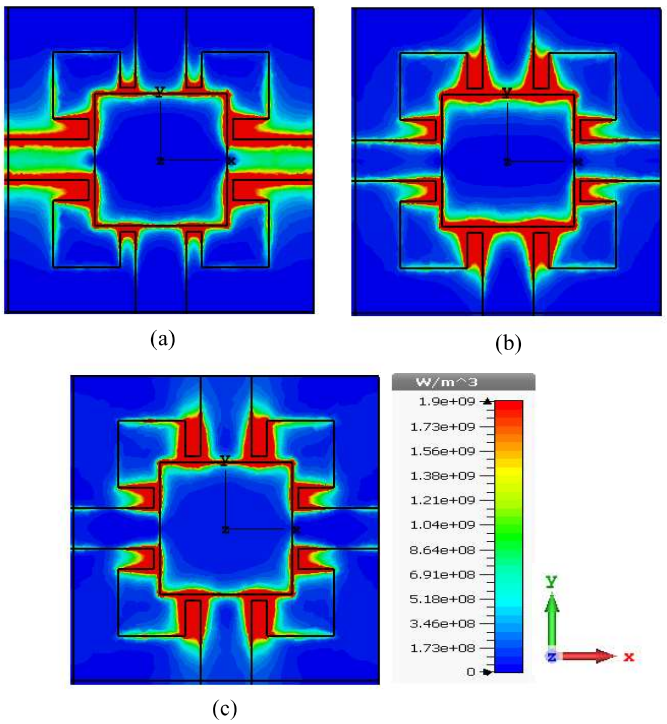

Fig. 2.11. Power loss on the graphene based metasurface at (a) 4.21 THz, (b) 6.78 THz and (c) 9.27 THz.

between the metal ground plane and the top graphene layer, the power loss density patterns of the absorber are introduced in Fig. 2.11. At lower frequency (4.21 THz), the power loss density distributions are concentrated at the edges of the whole horizontal slot of the graphene metasurface. At 6.78 THz, the power loss distributions are almost equally dispersed but partly on the edges of both the horizontal and vertical slots of the graphene layer. The power loss density is further enhanced in a denser way on the edges of both the horizontal and vertical slots of the top layer at 9.27 THz. It has been found that the power loss density distributions are identical for both TE and TM polarized electromagnetic waves.

Table 2.3. Comparison with Existing Graphene Metasurface Absorbers

Graphene based absorbers	**Fractional bandwidth**	**Frequency region (THz)**	**Thickness**	**Period of unit cell**
Liu et. al. [233]	37.79 %	7-10.2	~λ/8	~λ/14
Huang et. al. [227]	13.37 %	80-95	~λ/14	~3λ/4
He et. al. [234]	60 %	2-4	~λ/24	~λ/14
Fu et. al. [235]	28.26 %	5.5-9.5	~λ/5	~λ/11
In this report	90.34 %	3.69-9.77	~λ/11	~λ/13

Graphene Based Metasurface with Near Unity Broadband Absorption in the Terahertz Gap

Next, a design on graphene-based stacked metasurface has been proposed, which composes of three consecutive layers arranged on top of each other. A 2.5 µm thick amorphous silicon dioxide (SiO_2) is sandwiched between two graphene layers. A 1 nm thick modified fractal graphene pattern is deposited on the top surface of the amorphous SiO_2. On the other hand, a square-shaped graphene pattern of the identical thickness completely covers the backside of the SiO_2. Absorption bandwidth of 9.74 THz ranging from 2.06 THz to 11.80 THz has been achieved when the EM wave is incident on the top surface of the structure. A number of upcoming application bands can be sheltered in this whole bandwidth, which could be highly beneficial to modern wireless communications, including 5G communications and beyond. The design is ultra-thin in nature in terms of thickness and periodicity of a single unit cell.

2.4. Design and Simulation of Structure

The unit cell of the whole structure is depicted in Fig. 2.12. The top view, perspective view, and back view of the unit segment are illustrated in Fig. 2.12(a), Fig. 2.12(b), and Fig. 2.12(c), respectively. The whole structure of the unit cell consists of three consecutive layers where a modified-fractal type graphene pattern is deposited on top of the 2.5 µm thick amorphous silicon dioxide (SiO_2) substrate ($\varepsilon_r = 3.9,\ tan\,\partial = 0.0006$). The bottom side of SiO_2 is entirely covered with continuous graphene layer and the top graphene pattern is oriented along *x-y* plane. The open boundary is perpendicular to the top layer and is oriented along *z*-direction to allow electromagnetic wave (EM) approaching towards the top surface. In the terahertz region, the skin depth (δ_g) of graphene is negligibly small. Therefore, 1 nm thick graphene sheet is sufficient enough to interact with incoming EM wave [236].

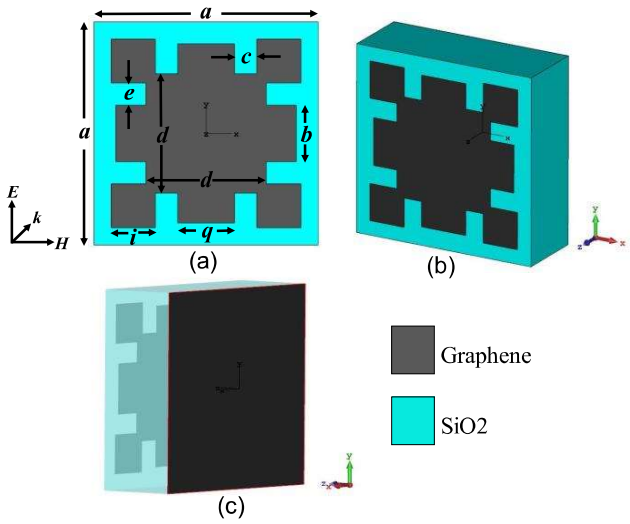

Fig. 2.12. (a) Top view, (b) 3-D perspective and (c) back view of the wideband graphene-based metasurface absorber in lower MIR region (a = 6.7 µm, b =1.8 µm, d = 3.8 µm, c = 0.9 µm, e = 0.9 µm, i = 1.4 µm, q = 1.8 µm).

The quantum capacitance is neglected here because of the thick dielectric substrate [236]-[237]. The DC electrostatic bias (E_o) is derived by considering the undoped and ungated case, i.e., μ = n_s = 0 in the equation (1.10), which gets modified in the form of equation (1.11) where ε_b is the dielectric constant of a substrate presented in the equation $D_n = \varepsilon_b E_o = en_s/2$. D_n denotes the normalized component of displacement vector on either side of a charged sheet in a homogeneous dielectric substrate having dielectric constant ε_b [236]-[237]. The maximum chemical potential μ_{max} can be calculated from equation (1.12), as presented in equations (1.13) and (1.14) where E_{bd} is the breakdown voltage of the dielectric substrate. In case of SiO_2, E_{bd} value is considered as ~ 1.5 V/nm and ε_r= 3.9 [236]-[237].

The propagation of a plane wave through a dielectric medium can be interpreted as an equivalent transmission line as shown in Fig. 2.13. Here, Z_o and Z_h are the characteristic impedances of free space and silicon dioxide (SiO_2) substrate, respectively. Z_{in} is the effective input impedance of the proposed graphene-based absorber. The top layer patterned graphene sheet acts as a conductive film having an equivalent impedance of Z_g. The substrate with

relative permittivity of ε_p is modeled as a transmission line of length h (h = substrate height). The input surface impedance of the dielectric is denoted as Z_1, which is expressed by equation (2.2) where β is the wave propagation constant in the dielectric substrate. The reflection coefficient (Γ) and the impedance of the graphene patch (Z_g) can be found from the equations (2.3) to (2.5). The complex surface conductivity of graphene in the lower terahertz region (0.1-10 THz) can be interpreted in terms of derivation as well as in the graphical form illustrated in [237]-[238].

$$Z_1 = jZ_h \tan(\beta h) \qquad (2.2)$$

$$\frac{1}{Z_{in}} = \frac{1}{Z_g} + \frac{1}{Z_1} \qquad (2.3)$$

$$\Gamma = \frac{Re[Z_{in}] - Z_o}{Re[Z_{in}] + Z_o} \qquad (2.4)$$

$$Z_g = \frac{1}{\sigma_g} \qquad (2.5)$$

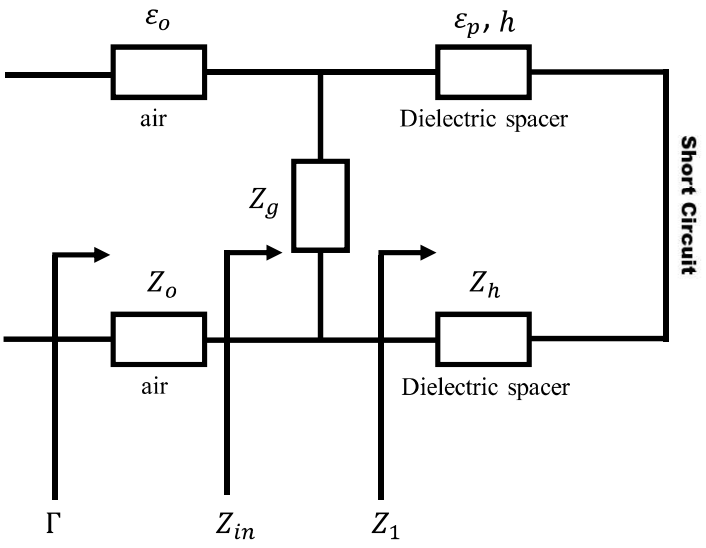

Fig. 2.13. Equivalent circuit schematic of the proposed absorber structure.

EM wave will have its different angular incidence on the proposed metasurface structure, including normal incidence. The top layer patterned graphene acts as a conductive film having an equivalent impedance $Z_g = R + jX$ where R and X are equivalent resistance and reactance of the patterned graphene metasurface acting as an interface between two different dielectric materials of air and SiO_2 helping to interact the incident EM wave into SiO_2 substrate; thereby giving rise to light-matter interaction. The coupling has been found to be improved between the top and bottom layer graphene, which is discussed in the next section of the chapter.

The unit cell is designed with infinite periodic boundary condition using CST Microwave

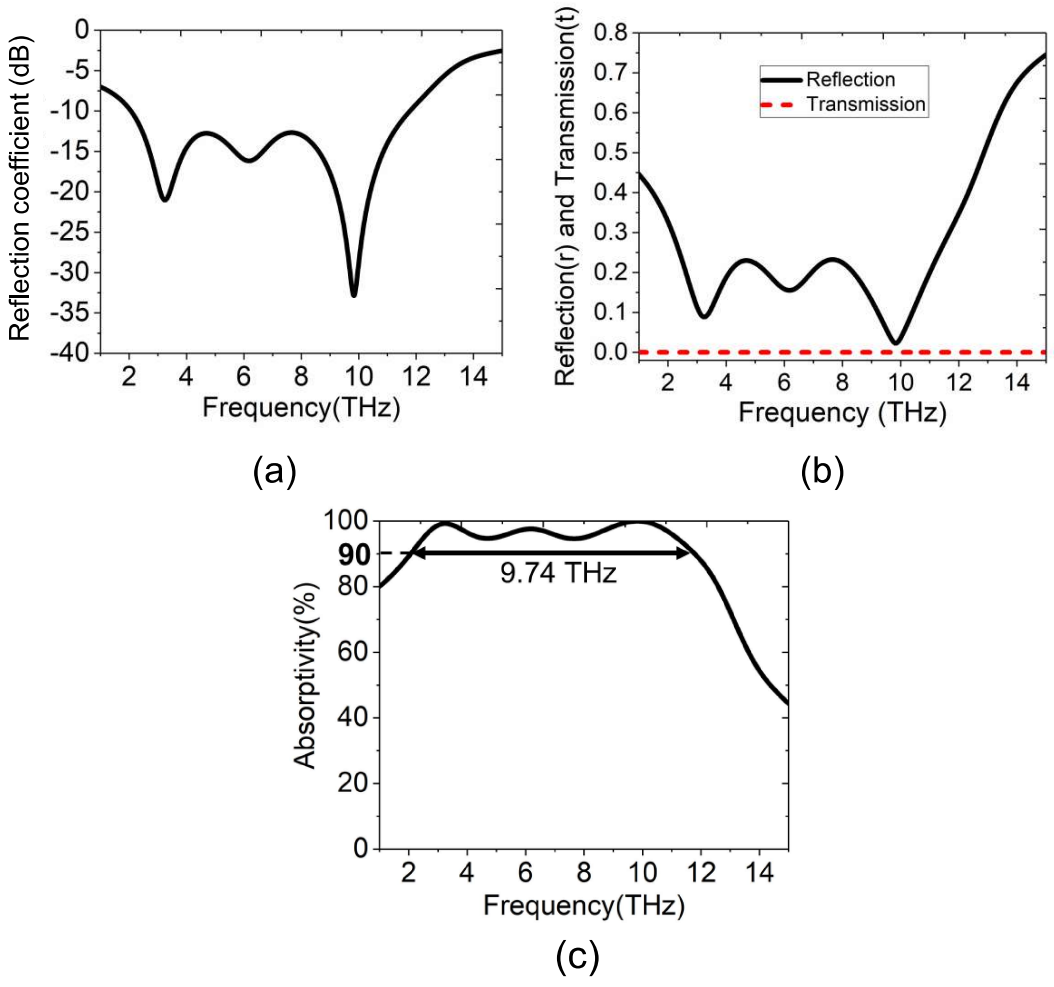

Fig. 2.14. Frequency responses of (a) reflection coefficient (r) and (b) reflection and transmission (t) co-efficients and (b) absorptivity (A) of the absorber structure in Fig. 1.

Studio software to realize the structure. The optimized parameter dimensions are described in Fig. 2.12. The design is explored in a systematic manner using the frequency domain solver to generate reflection (r) and transmission (t) coefficients. The absorption takes place not only due to the multiple reflections and superposition of EM wave but also due to the occurrence of multiple plasmonic coupling between two closely spaced graphene layers. The absorption is dependent only on the multiple reflections and superposition of EM wave between top graphene and bottom gold layer in the conventional case.

Graphene can be modeled as a thin metal sheet with the plasma frequency depending upon the Fermi level as provided in equation (2.6) [238]-[241]. The resonance frequency in graphene increases with the Fermi energy, which indicates that graphene exhibits "more-metallic"-type conductivity than semiconductor-type [105]. Therefore, a structured graphene metamaterial further provides wide absorption bandwidth by incorporating plasmonic resonance [242].

$$\omega_p = \left[\frac{2e^2 k_B T}{\pi\hbar^2 \varepsilon_o \Delta} ln\left\{2cosh\frac{E_f}{2k_B T}\right\}\right]^{\frac{1}{2}} \qquad (2.6)$$

The reflection coefficient (r) and negligible (zero) transmission coefficient (t) responses are plotted in Fig. 2.14(a) and Fig. 2.14(b), respectively. In the terahertz region, the bottom graphene layer at a certain chemical potential value (μ), can work as a metallic reflector supporting multiple plasmon resonances, and henceforth the transmission is zero as evident from Fig. 2.14(b) [105]. The metasurface covers a wide absorption bandwidth of 9.74 THz between 2.06 THz and 11.80 THz as the reflection level is under -10 dB within this whole range as evident from Fig. 2.14(a). The transmission spectra $|t|$ is equal to 0 in linear scale. So, the proposed sandwiched structure with two differently patterned graphene layers in two opposite sides of a silicon dioxide (SiO_2) block provides wideband absorption characteristics in the lower terahertz region with (almost) zero transmission. The absorptivity response is plotted in Fig. 2.14(c). The fractional bandwidth of 140.86% with respect to the center

frequency with more than 90% absorptivity has been realized. The reflection curve contains three resonance dips at 3.25 THz, 6.16 THz and 9.83 THz respectively. These resonance dips give rise to respective absorptivities of 99.9%, 97%, and 99.9%.

The as-presented three-dimensional (3D) geometry has three stacked layers. The top graphene decoration is mainly a modified fractal shape geometry. An additional plus-shaped graphene layer is superimposed with the conventional fractal-shaped graphene layer. This combined geometry has been chosen as it utilizes the available planar area of a circle of the maximum radius that can be enclosed within the periodicity of the unit cell most efficiently [243]. This newly-designed graphene layer will produce more coupling when it is analyzed with the periodic boundary condition, which is same as the practical situation during fabrication of the design. All the dimensions of the modified fractal-shaped geometry are parametrically optimized to improve the absorption bandwidth in the 'Terahertz Gap' region.

2.5. Design Evolution of the Structure

The evolution process of the finalized geometrical design has been inked in a step-by-step fashion in Fig. 2.15. The primary design has been undergone a number of modifications to be a potential graphene-based broadband metasurface absorber. The performance of corresponding absorptivities of the above said development of the top surface graphene patterns is illustrated in Fig. 2.16(a). The best absorptivity response can be achieved for the top geometrical shape of the graphene pattern shown in Fig. 2.15(g) due to the strong plasmonic coupling between the top and bottom graphene layers. In this case the graphene pattern has the largest electrical surface area to interact with the SiO_2 substrate effectively [244]. The square-shaped graphene pattern provides unity absorption in high frequency (10 THz). The fractal one has a unity absorptivity response in low frequencies. The square-shaped graphene geometry is also optimized with the two graphene arms to check absorptivity response with less complexity

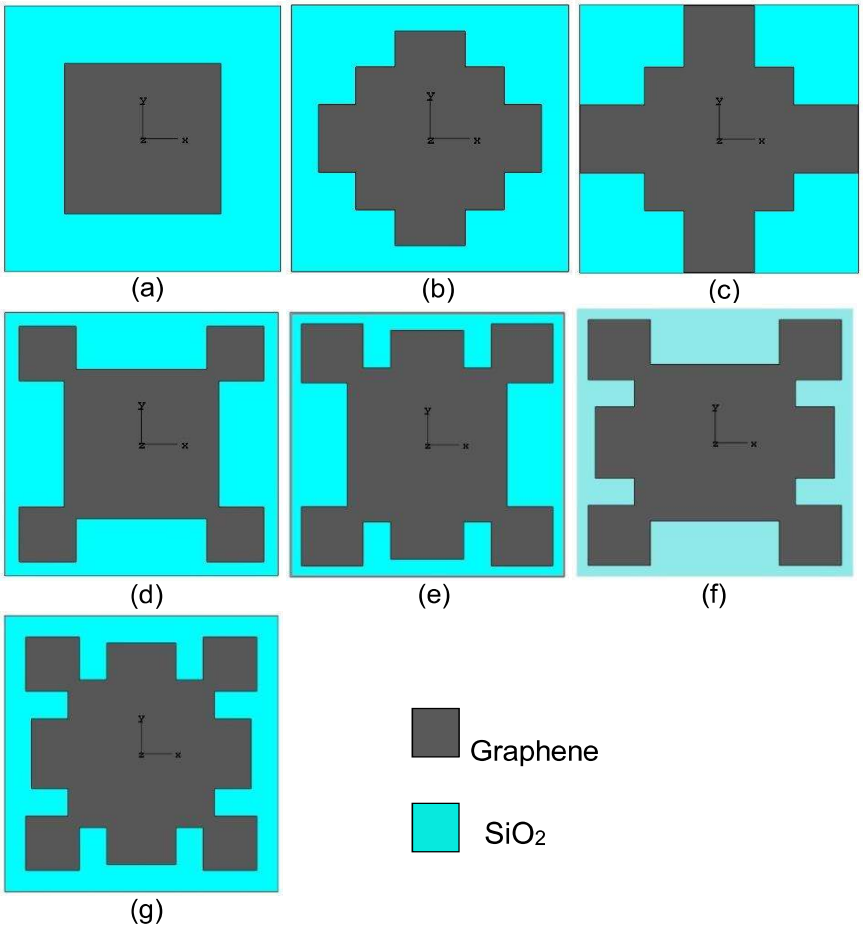

Fig. 2.15. Development of the final structure through different shapes of (a) only square, (b) square patch with optimized both arms, (c) square patch with optimized both arm's length upto periodicity, (d) only fractal (e) fractal with vertical arm (f) fractal with horizontal arm and (g) fractal with both arms.

in design. But the absorptivity is not as much enhanced as the fractal geometry with both arms. It can be observed from the additionally attached information in Fig. 2.16(a). The fractal geometry with two orthogonal graphene arms is optimized together to have the best absorptivity response possible within the overall design geometry (periodicity). The fractal shaped graphene patch along with the two arms provides significantly wider absorption bandwidth in comparison to the square-shaped graphene patch loaded with the two arms as shown in Fig. 2.16(a). The additional two geometries regarding top layer graphene pattern are also included in Fig. 2.16(b) and Fig. 2.16(c) respectively. Further, the bottom graphene layer

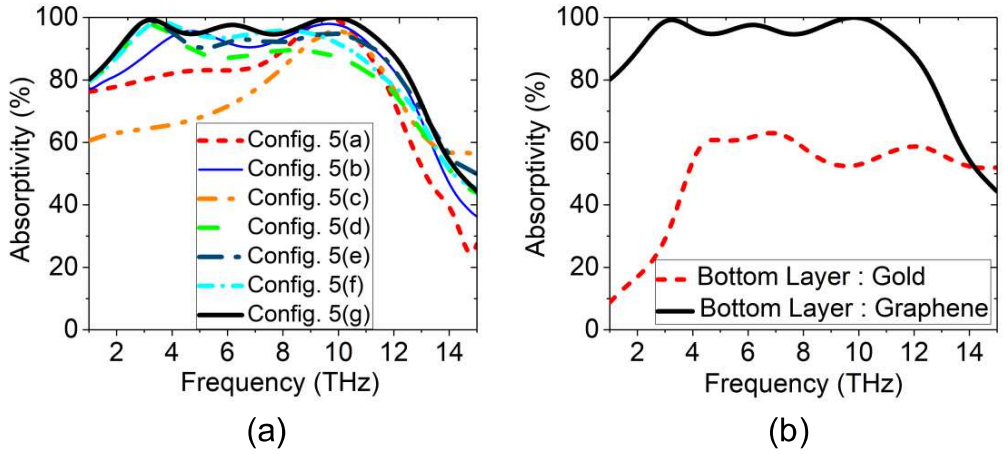

Fig. 2.16. Frequency responses of (a) different structural formations of top graphene layer keeping the bottom graphene layer shape constant and (b) the final structure with gold bottom layer in replacement of the continuous graphene layer.

of the optimized 3D geometry is replaced by 0.1 μm thick gold layer to compare the performance of both designs as depicted in Fig. 2.16(b). The proposed absorber with bottom graphene layer provides the better absorptivity response as additionally, pattern combination which is absent from the top graphene pattern and bottom metallic gold layer configuration [244].

2.6. Simulated Results and Discussions

A detailed discussion about all the structural and chemical parameters of the proposed design is an essential part of this study. The middle square graphene layer of the primitive fractal pattern is attached with four small and equal size corner square graphene pattern in such a way that the effective electrical length is maximum [243]. During the optimization process, one single geometrical dimension variable has been changed at a time keeping the other dimensions constant. The change in dimension of the middle square graphene pattern denoted as *d* can be interpreted as the variation in the effective electrical length of the overall top layer graphene geometry when the four similar small corner graphene blocks are constant at their positions. The best possible outcome can be viewed from Fig. 2.17(a) in terms of absorption bandwidth

with maximum absorptivity when d = 3.8 µm. The substrate height (h) plays a vital role in designing metasurface based absorber. The whole 3D structure works as a rectangular cavity in which EM wave enters into it through the top surface and gets reflected from the bottom surface with multireflection demonstrated by Fabry-Perot resonance [244]. In this case, the coupling between the top and bottom graphene layers adds more to the plasmonic resonance bandwidth resulting in high absorption in the previously said frequency range [105], [239]. The coupling is highest at h = 2.5 µm and the absorptivity response has three resonance peaks in this case which is clear from Fig. 2.17(b). The width (q) of the top layer plus-shaped graphene pattern, which is superimposed with the primitive fractal pattern has been undergone several variations. The best absorptivity response has been found for q = 1.8 µm in Fig. 2.18(a). The reason behind this response can be explained through the effective electrical length concept as well as strong capacitive coupling effect [245], [246]. It can be determined from Fig. 2.17(a) and Fig. 2.17(b) that the variations in absorption bandwidth have also been occurred because of the change in coupling strength between the resonating parts of the overall structure.

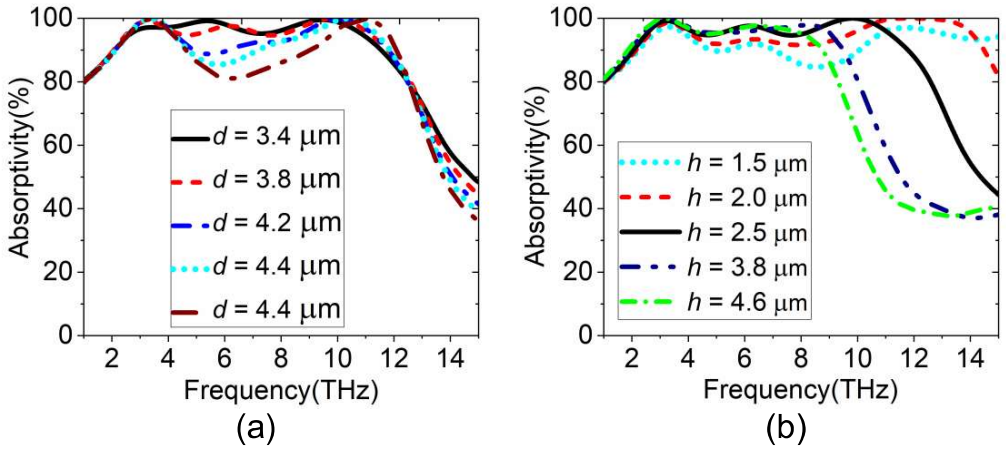

Fig. 2.17. Variations of absorptivity (a) for the variation of middle square graphene geometry (d) and (b) due to the change in substrate thickness (h) of the unit cell.

Chemical potential (μ) can control the Fermi level of graphene layer and as evident from equation (1.5). Two graphene layers are associated with this particular design. If external DC

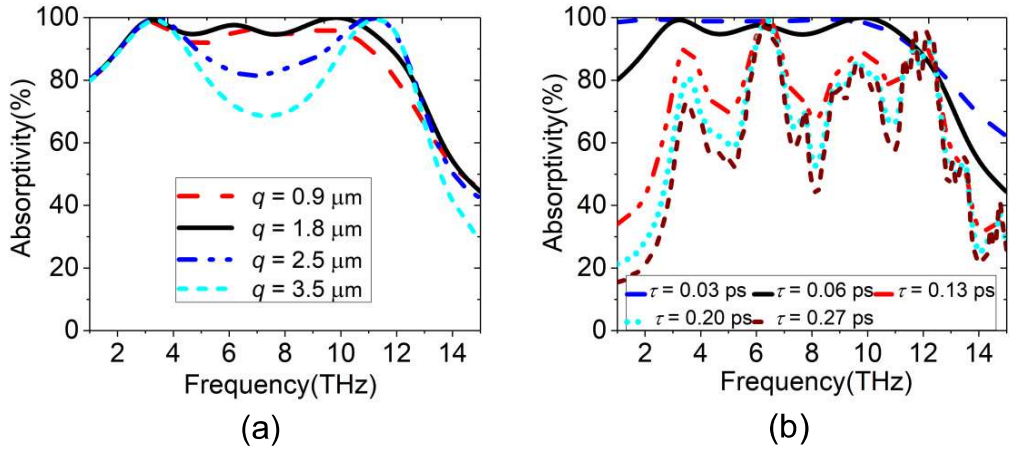

Fig. 2.18. Variations of absorptivity under (a) width variation of plus geometry of graphene layer (q) along with (b) the relaxation time (τ) variation.

bias has been applied between the two layers, the chemical potential will be altered accordingly. In this configuration, one single graphene layer works as an alternative gate to the other simultaneously [246]. In this case, the thickness of the substrate has its major role and it should be of optimized value so that the coupling between the top and bottom graphene layers will be maximum, which has been discussed in Fig. 2.17(b). This manuscript has discussed the alteration of μ for both the top and bottom graphene layers but single at a time. The chemical potentials of the top layer graphene and the bottom layer graphene are expressed as T_μ and B_μ respectively. The absorption bandwidth becomes tunable under this parametric variation. The absorptivity response shows red-shift in its spectral domain with the increase of T_μ while B_μ remains constant. The absorption bandwidth undergoes blue-shift with the increase of B_μ keeping T_μ invariant. The overall effect of the change of chemical potentials on the two different graphene surfaces has been depicted in Fig. 2.19(a) and Fig. 2.19(b) consecutively. The variations of chemical potential in the manuscript are realistic and it can be validated from the literature [247]-[248]. The spatial structure and thickness of the graphene layer are significant to the performance of the proposed metasurface absorber structure. By shaping the graphene structure in different dimensions results in the tailoring of the localization of electromagnetic

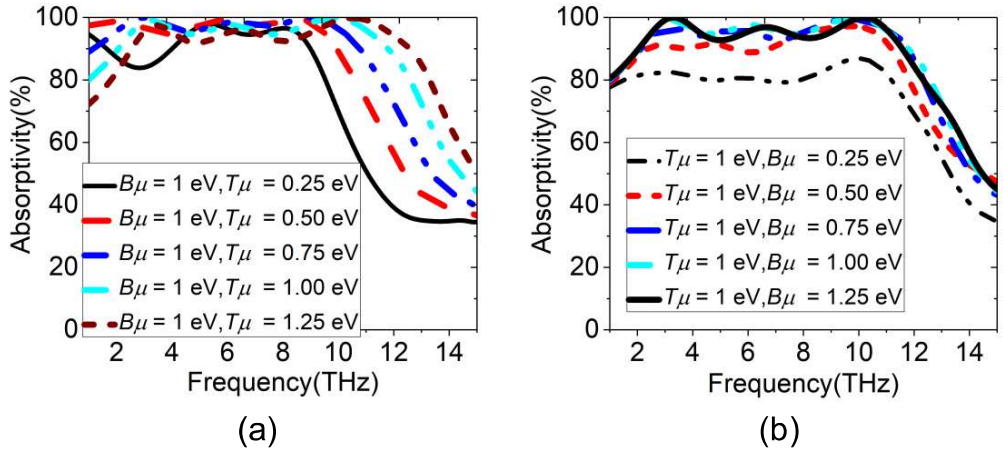

Fig. 2.19. Variations of absorptivity under (a) different values of top layer chemical potential ($T\mu$) and (b) bottom layer chemical potential ($B\mu$).

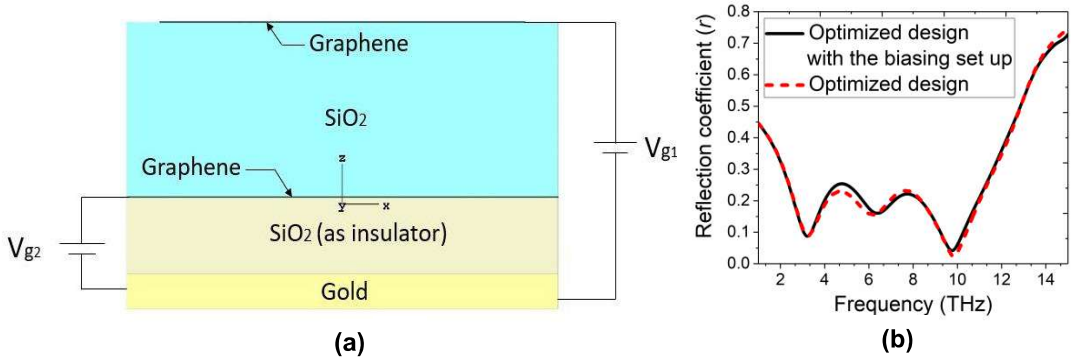

Fig. 2.20. (a) Configuration of the proposed structure with the biasing setup and (b) Comparison of reflection (r) coefficient of the structure with and without the biasing setup.

fields at the nanoscale [242], [249]. Fig. 2.20(a) shows a schematic diagram illustrating the various layers and to bias the graphene layers. Graphene's surface conductivity can be modulated by applying external DC biasing. The DC biasing can be applied to the structure for practical realization of control of μ as shown in Fig. 2.20(a). A common gate made of gold is introduced with the addition of a silicon dioxide (SiO_2) substrate placed just underneath the proposed graphene-based design. The conductivity of the two graphene layers can be controlled separately at a time by applying two different gate voltages V_{g1} and V_{g2} in between the graphene layers and the bottom gating gold structure to exploit T_μ and B_μ respectively [246], [250]. The additional two components yield no effect on the absorption characteristics as there is no transmission from the backside of the primarily designed proposed graphene-based

absorber design as seen from Fig. 2.20(b). The continuous bottom layer of graphene acts as a reflector in a particular frequency-band in the terahertz (THz) region by changing the chemical properties of the graphene. The surface conductivity of graphene is more in case of continuous graphene [105]. The chemical potential (μ) of both the graphene layers in the proposed geometry can be varied separately at a time by the biasing scheme shown in Fig. 2.20(a). Now, when the chemical potential value of the bottom layer is increased, the bottom continuous

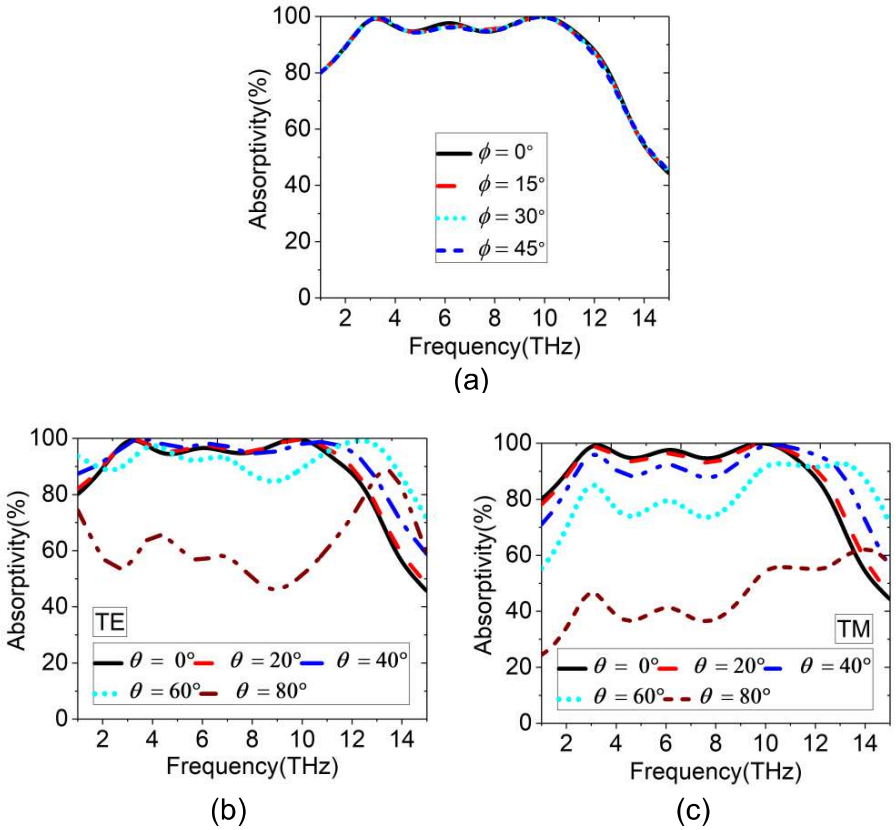

Fig. 2.21. Absorptivity responses under different (a) polarization angles and different incident angles (θ) for (b) TE polarization and (c) TM polarization.

graphene pattern is switched to a good reflector [105]. The bottom layer continuous graphene pattern of the proposed design works as a reflector when its chemical potential (μ) value is 1.25 eV. From the absorptivity response depicted in Fig. 2.21(a), it can be concluded that the proposed graphene-based metasurface is insensitive to incident polarization of EM wave owing to its four-fold symmetry. The structure is also examined under different incident

Table 2.4. Comparison with Existing Graphene Metasurface Absorbers

Graphene based absorbers	Fractional bandwidth	Frequency region	Thickness	Periodicity	Type	Max. Incidence angle (A >80%)
Liu *et. al.* [233]	37.79 %	7-10.2 THz	~λ/8	~λ/14	Single Layer	TE up to 60º TM up to 60º
H. Huang *et. al.* [18]	13.37 %	80-95 THz	~λ/14	~3λ/4	Single Layer	TE up to 65º TM up to 70º
S. He *et. al.* [234]	60 %	2-4 THz	~λ/24	~λ/14	Multilayer	Not discussed
P. Fu *et. al.* [235]	28.26 %	5.5-9.5 THz	~λ/5	~λ/11	Multilayer	TE beyond 65º TM up to 40º
A. Fardoost *et. al* [250]	88 %	0.5-5 THz	~λ/13	~λ/13	Multilayer	Not discussed
D. Chen *et. al* [251]	30 %	8.5-11.5 THz	~λ/2	~λ/2	Multilayer	TE beyond 30º TM up to 30º
F. Wang et. al. [256]	13.33 % & 9.52 %	7-8 THz, 10-11 THz	~λ/9	~λ/8	Single Layer	70º
Y. Zhang *et. al.* [253]	56%	25.08-44.81 THz	~λ/10	~λ/4	Single Layer	70º
L. L. Spada *et. al.* [254]	17.77%	210-240 THz	~λ/4	Not discussed	Multilayer	Multiband absorption up to 80º
Dong *et. al.* [255]	31.9%	2.58-3.56 THz	~λ/21	~λ/7	Multilayer	TE up to 40º TM up to 50º
Y. L. Xu et. al. [256]	26.6%	3-5 THz	~λ/4.3	~λ/12.5	Single Layer	TE up to 45º TM up to 60º
B. Z. Xu et. al. [257]	31.5%	0.5-3 THz	~λ/4.12	~λ/10.1	Multilayer	60º
M. Rahmanzadeh et. al. [258]	140%	0.55-3.12 THz	~λ/10	~λ/11	Multilayer	TE up to 40º TM up to 65º
E. S. Torabi et. al. [259]	66.7%	2-4 THz	~λ/8.33	~λ/6.7	Single Layer	Not discussed
K. Arik et. al. [260]	100%	0.5-1 THz	~λ/11.74	~λ/5.65	Single Layer	TE up to 60º TM up to 70º
X. Huang et. al. [261]	90%	1.23-2.73 THz	~λ/6.78	~λ/24.39	Single Layer	Not discussed
A. Khavasi et. al. [262]	100%	0.5-1.5 THz	~λ/11.76	~λ/4	Single Layer	Not discussed
Z. Su et. al. [263]	22.02%	9.7-12.1 THz	~λ/9.09	~λ/12.4	Single Layer	Not discussed
In this work	140.85831%	2.0625-11.80 THz	~λ/55.9	~λ/21.7	Single Layer	TE up to 60º TM up to 40º

angles (θ), including the normal incidence of the EM wave. The design produces above 90% absorptivity up to 60º incident angles in case of TE polarization of the EM wave and up to 40º incident angles in case of TM polarization under the optimized values of T_μ = 1 eV & B_μ= 1.25 eV in Fig. 2.21(b). This fact is confirmed from Fig. 2.21(b) and Fig. 2.21(c), respectively.

The electric field distributions are confined in nature at the horizontal corner edges of the modified fractal shaped top graphene layer at 3.25 THz as described in Fig. 2.22(a). At 6.16 THz, the electric field is concentrated on both horizontal and vertical edges of the top graphene layer demonstrated in Fig. 2.22(b). The E-field distributions at 9.83 THz are centralized at the vertical edges of the top graphene layer, and it is illustrated in Fig. 2.22(c).

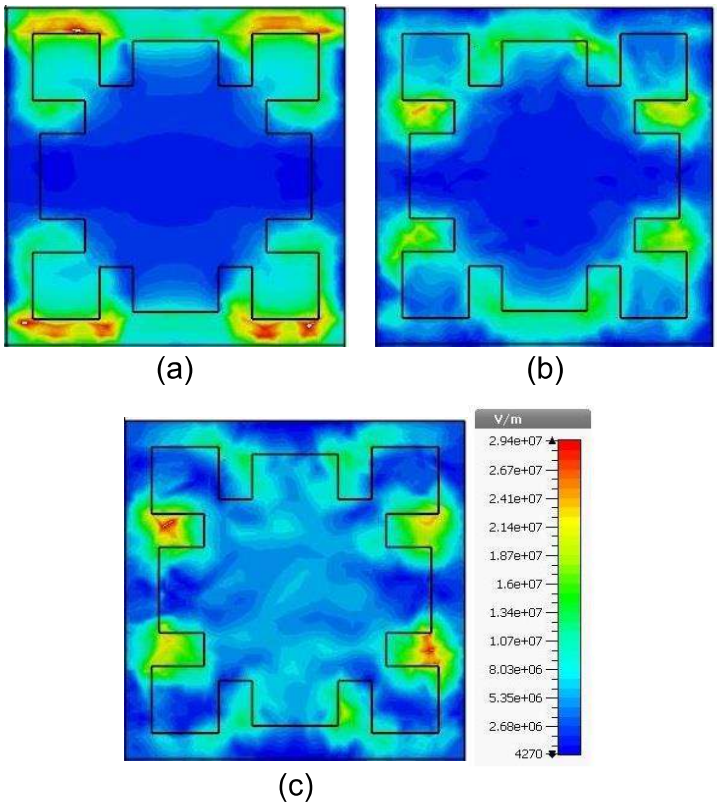

Fig. 2.22. (a) Electric field distributions at (a) 3.25 THz, (b) 6.16 THz and (c) 9.53 THz.

The surface current distributions can be indicative of the type of excitations associated with the resonance of any structure. To validate this concept, the current distributions of top and bottom

graphene layers are observed and discussed with the help of Fig. 2.23(a) and Fig. 2.23(b). The surface current distributions of the top and bottom graphene layers are anti-parallel defining magnetic excitation in view of resonance. Contrarily, at 9.83 THz the surface current distributions are of identical orientations; thereby forming electric excitation associated with resonance. The magnitudes of the surface current distribution are plotted also side by side at the aforementioned three different frequencies. The proposed modified fractal-shaped graphene metasurface with graphene back layer has many significant improvements over the previously published literatures presented in Table 2.4.

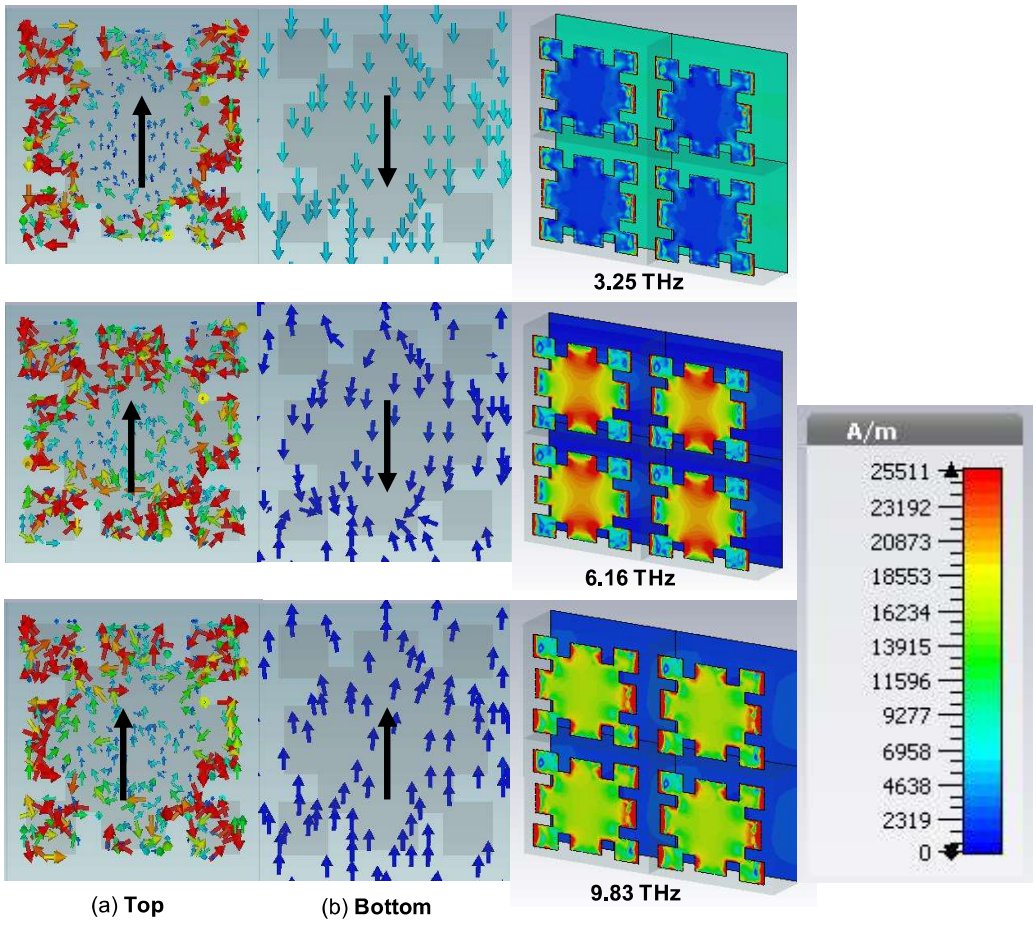

Fig. 2.23. Surface current distributions for (a) top layer and (b) bottom layer of proposed metasurface structure at 3.25 THz, 6.16 THz and 9.83 THz along with magnitude plot.

2.7. Conclusion

A graphene-based absorber for the lower mid-infrared region has been explored in this manuscript. We propose three layered structures consisting of top layer as patterned graphene structure, bottom layer as thin gold, and amorphous SiO_2 sandwiched in between them. The graphene layer is designed like a square fractal and then divided into four parts to have the four-fold symmetry to be polarization insensitive within a wide range of incidence angles up to 40º for both TE and TM modes of polarization. A square size layer is deposited in the middle of the fractal slotted and divided graphene pattern to increase coupling with each part. The designed prototype has been optimized through the modifications of several geometrical parameters. The structure offers more than 90% absorptivity over a fractional bandwidth of 90.34% with respect to the center frequency of the absorption band. The design is examined under the parametric variations of all the structural dimensions to check the best outcome possible. The absorptivity response can be tuned by changing the Fermi energy level of the graphene layer with the change of the chemical potential. The thickness of the designed absorber is $\sim\lambda/11$ with respect to lower frequency. The periodicity of the prototype is compact; being $\sim\lambda/13$ with respect to the lower frequency. The proposed absorber has many benefits over a number of existing literatures in terms of compactness, wide bandwidth achievement with a simple single layer graphene, and also for the lower MIR region.

In the second work, a graphene-based metasurface absorber has been designed covering an absorption bandwidth (more than 90% absorptivity) of 9.74 THz in between 2.06 THz and 11.80 THz within the whole 'Terahertz Gap'. The design is polarization insensitive as it exhibits four-fold symmetry. The design exhibits good performance in terms of absorptivity (80%) under different incident angles of the EM wave up to 60º angular stability for TE polarization and up to 40º angular stability for TM polarizations of EM wave. A primarily designed square fractal graphene layer is superimposed with a plus-shaped graphene surface

so that the electrical length of the complete structure is further improved and coupling between the top and bottom graphene layers gets stronger. The design offers above 90% absorptivity covering a fractional bandwidth of 140.86% with respect to the center of the absorption band. The structure is ultrathin with a thickness of around $\lambda/55.9$ with respect to the center of the whole absorption band. The structure is also compact having the periodicity approximately of $\lambda/21.7$. Proposed metasurface has significant improvements over the existing graphene-based metasurfaces and can cover the 'Terahertz Gap' mostly, which is very promising for terahertz communication, such as, 5G and beyond.